# Investigation of the modification of gold electrodes by electrochemical molecularly imprinted polymers as a selective layer for the trace level electroanalysis of PAH

Farah Ibrahim, Alexandre Sala, Armand Fahs, Aoife Morrin, Clément Nanteuil, Guillaume Laffite, Ian A Nicholls, Fiona Regan, Hugues Brisset, Catherine Branger

Electrochemistry Communications 169 (2024) 107837

Contents lists available at ScienceDirect

Electrochemistry Communications

journal homepage: www.elsevier.com/locate/elecom

# Investigation of the modification of gold electrodes by electrochemical molecularly imprinted polymers as a selective layer for the trace level electroanalysis of PAH

Farah Ibrahim [a], Alexandre Sala [a], Armand Fahs [a], Aoife Morrin [b], Clément Nanteuil [c], Guillaume Laffite [c], Ian A. Nicholls [d], Fiona Regan [b], Hugues Brisset [a], Catherine Branger [a,*]

[a] Université de Toulon, Laboratoire Matériaux Polymères Interfaces Environnement Marin (MAPIEM), Toulon, France
[b] School of Chemical Sciences, DCU Water Institute, Dublin City University, Glasnevin, Dublin 9, Ireland
[c] Klearia, 61 Avenue Simone Veil, CEEI Nice Côte d'Azur - Immeuble Premium, 06200 Nice, France
[d] Bioorganic & Biophysical Chemistry Laboratory, Department of Chemistry & Biomedical Sciences, Linnaeus University, SE-39182 Kalmar, Sweden

ARTICLE INFO

*Keywords:*
Molecularly imprinted polymers (MIPs)
Electrochemical sensor
Benzo(a)pyrene
Redox probe

ABSTRACT

Electrochemical molecularly imprinted polymers (e-MIPs) were grafted for the first time as a thin layer to the surface of a gold electrode to perform trace level electroanalysis of benzo(a)pyrene (BaP). This was achieved by controlled/living radical photopolymerization of a redox tracer monomer (ferrocenylmethyl methacrylate, FcMMA) with ethylene glycol dimethacrylate in the presence of benzo(a)pyrene as the template molecule. For that purpose, a novel photoiniferter-derived SAM was first deposited on the gold surface. The SAM formation was monitored by cyclic voltammetry and electrochemical impedance spectroscopy. Then, the "grafting from" of the e-MIP was achieved upon photoirradiation during a controlled time. Differential pulse voltammetry was used to quantify BaP in aqueous solution by following the modification of the signal of FcMMA. A limit of detection of 0.19 nM in water and a linear range of 0.66 nM to 4.30 nM, were determined, thus validating the enhancement of sensitivity induced by the close contact between the e-MIP and the electrode, and the improved transfer electron.

## 1. Introduction

Polycyclic aromatic hydrocarbons (PAHs) are environmental pollutants generated by anthropogenic activities such as industrialization, agriculture, and urbanization as well as by natural sources, like volcanic eruptions and natural forest fires [1]. People are constantly exposed to these substances, which can be detected in the air, soil, and natural water. Several PAHs are classified as hazardous pollutants, endangering both the environment and human health. These compounds tend to accumulate in the environment and the adipose tissue in the body for decades and exert toxic effects on various types of organisms in the ecosystem. Many PAHs have toxic, carcinogenic, and mutagenic properties. They are linked with chronic diseases such as cancer, respiratory diseases, neurodegenerative disorders, and cardiovascular diseases [2]. Among PAHs, benzo(a)pyrene (BaP) has been identified and classified as category 2A (probably carcinogenic) to humans by the International Agency for Research on Cancer. Therefore, the EU sets maximum levels for BaP in a range of foodstuffs, such as foods for infants and young children (less than 1 $\mu g.kg^{-1}$), fish (less than 2 $\mu g.kg^{-1}$), smoked meat and fish (less than 2 $\mu g.kg^{-1}$) and other food products [3,4]. High levels of PAHs have been abundantly found in natural water due to oil spills, microplastic pollution, and industrial and domestic waste discharges [5]. The EU requires maximum levels for BaP in drinking water and surface water as low as 0.01 μg/L [6] and 0.05 μg/L [7], respectively. Therefore, monitoring and control of environmental exposure to PAHs, particularly in natural water, is an urgent need. Over the past decade, a great deal of research has focused on real-time monitoring of pollutants in surface water and a number of devices have been designed for this purpose [8,9].

The integration of molecularly imprinted polymers (MIPs) as selective recognition receptors in sensing devices emerged as an innovative technique, allowing the detection of a wide range of analytes in different media [10,11]. MIPs possess robust molecular recognition abilities owing to their synthesis process [12]. These polymers can mimic the natural "lock and key" action of biological recognition elements, such as enzymes and antibodies [13–16]. However, these synthetic

* Corresponding author.
*E-mail address:* branger@univ-tln.fr (C. Branger).

https://doi.org/10.1016/j.elecom.2024.107837
Received 20 September 2024; Received in revised form 31 October 2024; Accepted 9 November 2024
Available online 12 November 2024

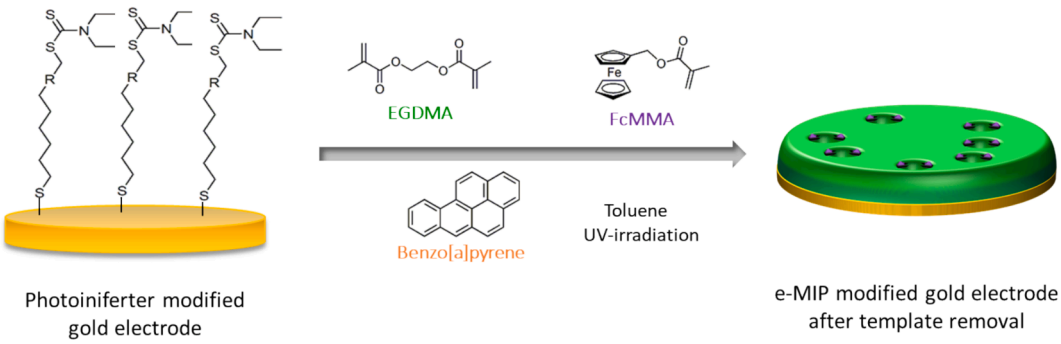


**Fig. 1.** Elaboration of e-MIP modified gold electrode.

macromolecules, contrary to their natural analogues, exhibit improved mechanical properties and higher stability in harsh environments, and can therefore be used at different temperatures, in different solvents and at different pH. Molecular imprinting consists, in the first step, of complexing one or more functional monomers and a crosslinking agent with an analyte (template). Then, the mixture is co-polymerized to obtain a highly cross-linked polymer. Vacant imprinted binding sites complementary to the template in terms of structure, size, and functionality are generated in the synthetic polymer after the template is removed. MIPs exhibit strong affinity and high selectivity for the target molecule and can thus recognize it in complex samples such as biological fluids and environmental samples. Another interesting property of these receptors is that they can be tailored to bind a large variety of targets through their selective binding sites by changing the template used in their synthesis.

Electrochemical sensing is one of the most powerful techniques for detecting a broad range of chemical species [17]. It offers high sensitivity, fast response, simple use, real-time measurement, and possible miniaturization [18]. However, this analytical tool often suffers from low selectivity toward the analyte. To address this issue, remarkable progress has been made in the last decade on electrochemical sensors coupled with MIPs as sensing elements [19]. For non-electroactive templates, like most organic molecules, an external electrochemical probe is required for the detection of target binding. However, this can be avoided by using an electroactive molecule as a functional monomer and internal electrochemical probe to detect target molecules that don't exhibit electrochemical redox activity. This is the principle of electrochemical molecularly imprinted polymers (e-MIP), which were first designed to detect BaP [20]. The concept has been extended to detect bisphenol A [21] and vancomycin [22]. The coupling of e-MIPs to electrochemical sensors allows direct screening of non-redox active molecules through a fast conversion of the molecular binding into an electrochemical readout due to the presence of a redox molecule incorporated in the e-MIP [23,24].

Good analytical performance of a MIP-electrochemical sensor is dependent upon the sensing element. A MIP with high binding capacity, intense electrochemical signal and fast mass transfer provides high sensitivity and binding affinity to the sensor. MIPs can be incorporated into electrochemical sensors according to various approaches, some of which include electropolymerization methods, or modification of transducers surface by particles of MIPs, by drop-casting/coating strategies and surface imprinting method that allows to form thin films on the surface [11,25]. Growing ultrathin MIP films from the electrode surface offers the advantage of bringing the recognition element close to the transducer [26].

In this study, we present a method to design an e-MIP sensor for the detection of BaP as a marker of PAHs. During the e-MIP synthesis, the ferrocenylmethyl methacrylate (FcMMA) monomer was used as a redox tracer. Thanks to its aromatic rings, the FcMMA monomer can bind to BaP through π- π stacking interactions promoting good binding between the e-MIP and the template. The electroactive ferrocenyl probe is incorporated inside the e-MIP and promotes selective binding to the target and transforms this binding into an electrochemical signal, which allows polymer-template binding to be monitored through the reduction in ferrocene signal resulting from PAH rebinding. For that purpose, the surface of gold microelectrodes was modified by an original photoiniferter containing a thiol group able to form a self-assembled monolayer (SAM) on a gold substrate and possessing a dithiocarbamate function to initiate radical polymerization in the presence of the monomers once activated by UV light (Fig. 1). This SAM immobilized on gold was used to perform a surface-initiated controlled/living radical photopolymerization (CLRP) directly on the electrode surface through a "grafting from" procedure. CLRP mediated by a photoiniferter is an elegant technique of radical polymerization that promotes the synthesis of highly homogenous and well-defined polymers in terms of molecular weight, polydispersity, end functionality, chain architecture and composition [27]. In MIP synthesis, it allows the control of the polymerization and contributes to a homogenous dispersion of binding sites that ultimately leads to enhanced binding affinities and improved template recognition and diffusion across the polymer [28].

## 2. Experimental Section

### 2.1. Chemicals

Reagents and solvents were of analytical purity or better and used without any purification steps unless stated otherwise.

Benzo[a]pyrene (BaP, 96 %), 2-chloromethylphenylisocyanate (97 %), 6-mercapto-1-hexanol (97 %), potassium chloride (99.0–100.5 %), potassium ferricyanide ($K_3Fe(CN)_6$, 99 %), potassium ferrocyanide ($K_4Fe(CN)_6$, 99 %), sulfuric acid (98 %), silica gel (40–63 μm) were obtained from Sigma-Aldrich. Dibutyltin dilaurate (94 %), tri-*n*-butylphosphine (95 %), potassium iodide (KI), sodium diethyldithiocarbamate trihydrate (98 %), Iodine (>95 %), magnesium sulfate ($MgSO_4$, 99 %, anhydrous), toluene (99.5 %, anhydrous), tetrahydrofuran (THF, 99.5 %, anhydrous), chloroform (99 %, anhydrous), dichloromethane (+99 %), acetonitrile (99.7 %), acetone (≥99.5 %), methanol (≥99.8 %), ethanol (96 %) were purchased from Acros organic (Geel, Belgium).

Sodium sulfite anhydrous ($Na_2SO_3$, 98 %) and sodium chloride (NaCl, 99 %) were purchased from ThermoFisher Scientific.

Hydrogen peroxide (30 %w/v) was purchased from VWR Chemicals.

Ethylene glycol dimethacrylate (EGDMA, 98 %), purchased from Acros organic (Geel, Belgium), was washed with a 10 % NaOH solution and dried over $MgSO_4$ to remove polymerization inhibitors.

FcMMA was synthesized as previously described [29].

Aqueous solutions were prepared using MilliQ water (18.2 MΩcm, Merck Millipore Q-POD).

### 2.2. Instrumentations

$^1H$ and $^{13}C$ NMR spectra were obtained using a Bruker Advance 400-

MHz spectrometer (Bruker France).

AFM experiments were carried out on a Multimode 8 microscope (Bruker) using the PeakForce Tapping AFM mode (PFT). The scans were performed at different regions on a surface area of 1 μm × 1 μm and collected with 256 × 256 pixels at a scan rate of 0.8 Hz. The nominal spring constant of the used cantilever is 0.4 N/m (SCANASYST-AIR). The measurements were carried out under ambient conditions at room temperature to characterize the surface topography of the different samples.

### 2.3. Synthesis of the photoiniferter

#### 2.3.1. Synthesis of 6,6́-disulfanediylbis(hexane-1-ol) (2)

6-mercapto-1-hexanol (1.0 mL, 7.3 mmol) and KI (0.83 g, 5.0 mmol) were dissolved in 30 mL methanol. A methanolic solution of $I_2$ (0.27 M) was then added dropwise to the mixture while stirring until the solution color turned red. The mixture was stirred for one supplementary hour at room temperature. 4 mL of a saturated solution of $Na_2SO_3$ was added. Methanol was removed under vacuum. The crude was dissolved in 20 mL NaCl saturated solution, and then extracted three times with 50 mL dichloromethane. The organic phase was dried over $MgSO_4$ and concentrated under vacuum to obtain a colorless solid with 98 % yield (1.00 g, 3.60 mmol).

$^1$H NMR (400 MHz, $CDCl_3$, δ in ppm) $\delta$ 3.65 (t, $^3J$ = 6.5 Hz, 4H, 2 C$\underline{H}_2$-OH), 2.68 (m, 4H, 2 $CH_2$-S), 1.70 (m, 4H, 2 $CH_2$), 1.56 (m, 6H, 2 $CH_2$ and 2 OH), 1.40 (m, 8H, 4 $CH_2$).

$^{13}$C NMR (101 MHz, $CDCl_3$, δ in ppm) $\delta$ 62.99 ($CH_2$-OH), 39.30 ($CH_2$-S), 32.82 ($\underline{C}H_2$-$CH_2$-OH), 29.40 ($CH_2$), 28.52 ($CH_2$), 25.66 ($CH_2$). MP: 37.5 °C.

#### 2.3.2. Synthesis of 6-{[6-({[2-(chloromethyl)phenyl]carbamoyl}oxy) hexyl]disulfanyl}hexyl N-[2-(chloromethyl)phenyl]carbamate (3)

The obtained product (**2**, 1.01 g, 3.79 mmol) and 2-chloromethylphenylisocyanate (1.16 mL, 8.59 mmol) were dissolved in anhydrous chloroform under argon. The solution was cooled in an ice bath and dibutyltin dilaurate (260 μL, 4.84 mmol) was added. The mixture was stirred for 2 h at 0 °C and then for 96 h at room temperature. The crude reaction mixture was concentrated under vacuum and the product was purified on silica gel using 70/30: chloroform/acetone as eluent. A colorless solid (2.165 g, 3.60 mmol) was obtained with 95 % yield.

$^1$H NMR (400 MHz, $CDCl_3$, δ in ppm) $\delta$ 7.84 (d, $^3J$ = 7.9 Hz, 2H, $CH_2$-C=C$\underline{H}_{aromatic}$), 7.37 (m, 2H, 2 $CH_{aromatic}$), 7.28 (dd, $^3J$ = 7.6 Hz, $^4J$ = 1.5 Hz, 4H, 2 C$\underline{H}_{aromatic}$), 7.09 (td, $^3J$ = 7.5, $^4J$ = 1.2 Hz, 2H, 2 NH-C=C$\underline{H}_{aromatic}$), 6.90 (s, 2H, 2 NH), 4.62 (s, 4H, 2 $CH_2$-Cl), 4.19 (t, $^3J$ = 6.7 Hz, 4H, 2 $CH_2$-O), 2.69 (m, 4H, $CH_2$-S), 1.71 (m, 8H, 4 $CH_2$), 1.43 (m, 8H, 4 $CH_2$).$^{13}$C NMR (101 MHz, $CDCl_3$, δ in ppm) $\delta$ 153.31 (C=O), 136.10 ($C_{aromatic}$), 129.48 ($C_{aromatic}$), 129.39 ($C_{aromatic}$), 126.55 ($C_{aromatic}$), 123.72 ($C_{aromatic}$), 122.16 ($C_{aromatic}$), 64.90 $\underline{C}H_2$-O), 43.37 ($CH_2$-Cl), 38.26 ($CH_2$-S), 28.39 ($CH_2$), 28.12 ($CH_2$), 27.47 ($CH_2$), 24.87 ($CH_2$). MP: 114.5 °C.

#### 2.3.3. Synthesis of 6-{[(2-{[(diethylcarbamothioyl)sulfanyl]methyl} phenyl)carbamoyl]oxy}-1-mercapto-hexane (5)

The obtained product (**3**, 1.53 g, 2.55 mmol) and sodium diethyldithiocarbamate (1.68 g, 7.45 mmol) were dissolved in anhydrous THF. The mixture was heated to 40 °C in the dark for 23 h. The reaction mixture was left to cool down and the solvent was evaporated under vacuum. 100 mL of dichloromethane was added to dissolve the crude, and the organic phase was extracted 3 times using 20 mL of NaCl saturated solution and dried over $MgSO_4$. Tri-*n*-butylphosphine (4.10 mL, 8.11 mmol) and milliQ water (93 μL, 5.1 mmol) were then added under argon and the mixture was stirred 24 h at room temperature. Dichloromethane was evaporated under vacuum and the reaction product was purified on silica gel using chloroform as eluent. (0.63 g, 1.53 mmol) of colorless oil was obtained with 60 % yield.

$^1$H NMR (400 MHz, $CDCl_3$, δ in ppm) $\delta$ 7.94 (d, $^3J$ = 8.0 Hz, 1H, $CH_2$-C=C$\underline{H}_{aromatic}$), 7.66 (s, 1H, NH), 7.27 (m, 2H, 2 $CH_{aromatic}$), 7.02 (td, $^3J$ = 7.7 Hz, $^3J$ = 7.9 Hz, $^4J$ = 1.2 Hz, 1H, NH-C=C$\underline{H}_{aromatic}$), 4.66 (s, 2H, Ar-C$\underline{H}_2$-S), 4.15 (t, $^3J$ = 6.6 Hz, 2H, $CH_2$-O), 4.04 (q, $^3J$ = 7.1 Hz, 2H, C$\underline{H}_2$-$CH_3$), 3.73 (q, $^3J$ = 7.1 Hz, 2H, C$\underline{H}_2$-$CH_3$), 2.56 (q, $^3J$ = 7.4 Hz, 2H, C$\underline{H}_2$-SH), 1.66 (m, 4H, 2 $CH_2$), 1.44 (m, 4H, 2 $CH_2$), 1.37 (t, $^3J$ = 7.8 Hz, 1H, SH), 1.32 (t, $^3J$ = 7.2 Hz, 3H, $CH_3$), 1.29 (t, $^3J$ = 7.1 Hz, 3H, $CH_3$).

$^{13}$C NMR (101 MHz, $CDCl_3$, δ in ppm) $\delta$ 194.57 (C=O), 154.30 (C=S), 136.74 ($C_{aromatic}$), 130.89 ($C_{aromatic}$), 128.70 ($C_{aromatic}$), 125.73 ($C_{aromatic}$), 123.61 ($C_{aromatic}$), 121.56 ($C_{aromatic}$), 65.08 ($CH_2$-O), 50.11 ($CH_2$-N), 46.99 ($CH_2$-N), 39.14 ($CH_2$-S), 33.92 ($CH_2$-SH), 28.82 ($CH_2$), 28.01 ($CH_2$), 25.40 ($CH_2$), 24.55 ($CH_2$), 12.52 ($CH_3$), 11.59 ($CH_3$).

### 2.4. Photoiniferter SAM formation on gold electrodes

The gold electrodes were manufactured in an ISO 6 cleanroom by Klearia company, Nice, France. Briefly, the electrodes were coated on a flat glass substrate (4'' wafers/ D263 material /1 mm thickness) through a lithography mask by a sublimation process thanks to a high energy electron beam inside a vacuum evaporation chamber.

The electrodes are composed of an intermediate 20 nm Titanium layer specifically coated to promote a strong adhesion on the glass substrate and covered with a 100 nm gold layer. In a last step, the glass wafer containing several features was diced in individual electrode units of dimensions about 26x2.4 mm.

To clean the surface of the electrodes, these were first washed in acetone, ethanol and MilliQ water for 10 min each. Then, they were immersed in a freshly prepared piranha solution (70/30: $H_2SO_4$ (96 %) / $H_2O_2$ (30 %w/v)) for 15 min, and were rinsed with a large amount of MilliQ water and dried using argon. After the treatment, each electrode was immersed in a 0.5 M solution of $H_2SO_4$ and was cycled from −0.3 to 1.5 V (*vs* SCE) at a scan rate of 100 mV/s until a steady state was reached.

For the SAM modification, the electrodes were immersed in the freshly prepared 0.24 M photoiniferter in THF solution for 24 h at +4 °C. The modified electrode was rinsed with THF to remove any unbound molecules and was dried with an argon flow.

### 2.5. Grafting polymer from the electrode surface

Electrodes modified with the photoiniferter were later immersed in a mixture of BaP (0.0097 g, 38.6 μmol, 1 eq), FcMMA (0.0551 g, 193 μmol, 5 eq), EGDMA (185 μL, 980 μmol, 25 eq) and 150 μL toluene and irradiated for 4 h with a 365 nm-UV lamp (Vilber-Lourmat VL-8.L, 8 W) placed at 1 cm distance to synthesize the e-MIP. To remove the template and unreacted monomers, the modified electrodes were washed with toluene, acetonitrile, acetone and water for 10 min each. The non-imprinted polymer (e-NIP) that serves as a reference was synthesized using the same conditions as for the MIP, but without BaP.

### 2.6. Characterization of the grafting

Surface modification of gold microelectrodes was followed by cyclic voltammetry (CV), electrochemical impedance spectroscopy (EIS) and AFM.

All electrochemical measurements were performed using a three-electrode system, where the modified gold electrode was used as the working electrode, a saturated calomel electrode (SCE) and a platinum (Pt) wire were used as the reference and the counter electrodes respectively (purchased from ALS Japan).

For CV and EIS measurements, an equimolar mixture of $[Fe(CN)_6^{4-}]$/ $[Fe(CN)_6^{3-}]$ (1 mM) was used in aqueous KCl (0.1 M) as supporting electrolyte. CV measurements were performed at room temperature using Metrohm Dropsens potentiostat *μ*Stat 8000 controlled with the DropView 8400 software package. CV measurements were carried out from −0.2 V to 0.6 V at a step potential of 10 mV and a scan rate of 100 mV/s.

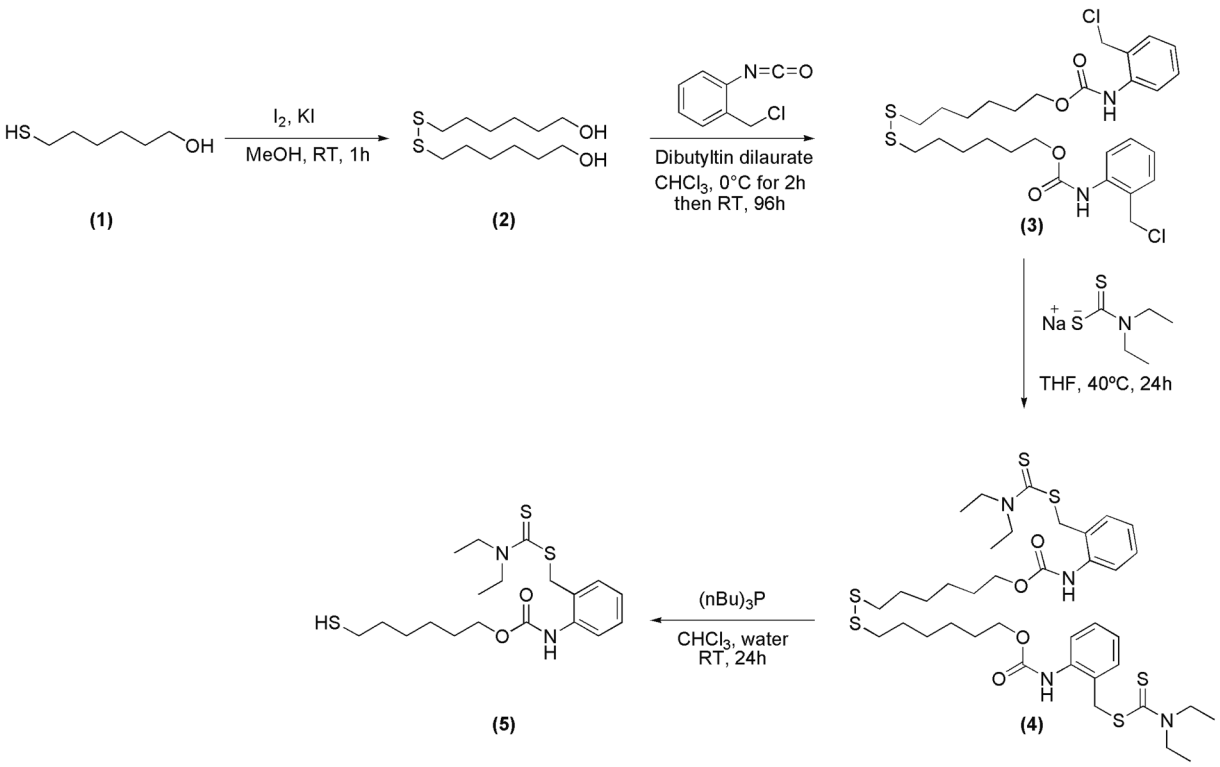


**Fig. 2.** Synthesis of the photoiniferter.

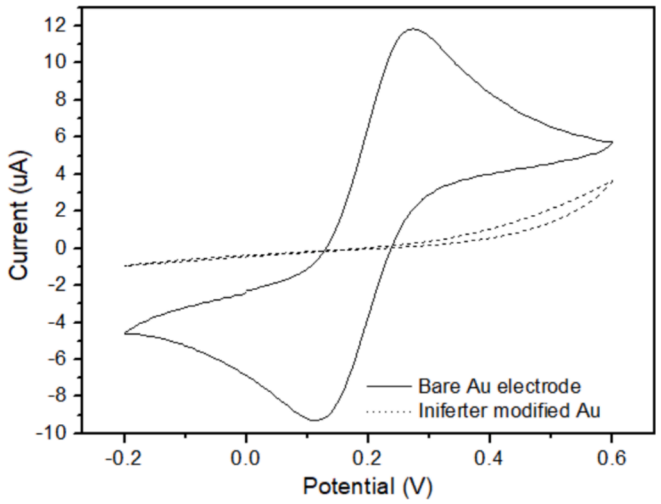


**Fig. 3.** Cyclic voltammograms carried out in 10 mM $[Fe(CN)_6^{4-}]/[Fe(CN)_6^{3-}]$ in 0.1 M KCl using bare and the photoiniferter modified gold electrodes. SCE reference electrode. V = 100 mV/s.

Impedance measurements were carried out at room temperature with a BioLogic VSP-300 potentiostat and spectra were treated using EC-Lab software. Impedance spectra were acquired at frequencies that ranged from 0.1 Hz to 1 MHz, applying a potential of 0.2 V and an amplitude of 0.01 V. Data evaluation was performed using Nyquist plots.

### 2.7. Evaluation of the electrode performances

Differential pulse voltammetry (DPV) was used to evaluate the polymer-coated electrodes proprieties. The measurements were carried out in a 5 mL electrochemical cell using aqueous KCl solution (0.1 M) as electrolyte at room temperature using Metrohm Dropsens potentiostat $\mu$Stat 8000 between 0 and 0.6 V, (pulse width: 10 ms, pulse amplitude: 150 mV, step E: 10 mV, scan rate: 0.01 V $s^{-1}$). The potentiostat and the electrodes used in these adsorption experiments are the same used in the CV experiments.

Differential pulse voltammograms of e-MIP modified electrode showed the anodic wave of the ferrocenyl redox group incorporated in the polymer. It was noted that the ferrocene peak stabilizes after performing at least 15 cycles of DPV, and then, the different voltammograms are superimposed.

## 3. Results and discussion

### 3.1. Modification of gold electrode by the photoiniferter

The synthesis scheme of the photoiniferter is shown in Fig. 2. The synthesis was performed following a modification of a reported procedure by replacing the 4-chloromethylphenylisocyanate with 2-chloromethylphenylisocyanate [30].

The formation of the photoiniferter SAMs on gold electrode surfaces was followed by cyclic voltammetry (CV) and electrochemical impedance spectroscopy (EIS) using the redox $[Fe(CN)_6^{4-}]/[Fe(CN)_6^{3-}]$ couple as the electroactive probe. CV is a simple technique for characterizing the conductive/insulative properties of the modified electrodes using redox couples as probes. Fig. 3 shows the cyclic voltammograms of bare gold and photoiniferter SAM-modified gold electrodes. In CV measurements, bare gold electrodes displayed the anodic and the cathodic waves corresponding to the redox couple $[Fe(CN)_6^{4-}]/[Fe(CN)_6^{3-}]$, implying that the electron transfer reaction is completely diffusion controlled. Whereas, these redox waves were no longer observed after the photoiniferter SAM formation on gold electrodes. This confirms that a highly ordered, compact monolayer of the photoiniferter is formed on the gold surface and the insulative properties of this monolayer completely block electron transfer at the electrode surface.

EIS was used to evaluate the quality of the coverage of the electrodes. Equimolar solutions of $K_3Fe(CN)_6$ and $K_4Fe(CN)6$ were used to

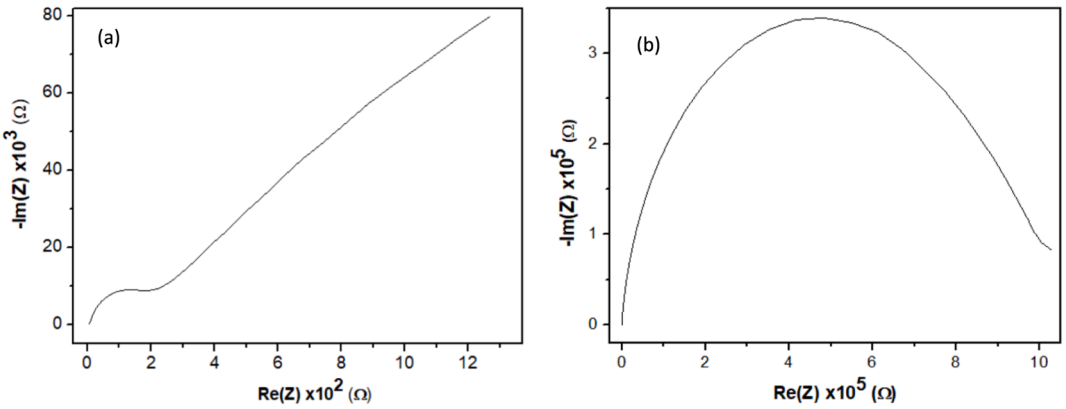


**Fig. 4.** Electrochemical impedance spectra recorded in 1 mM $[Fe(CN)_6^{4-}]/[Fe(CN)_6^{3-}]$ in 0.1 M KCl of (a) the bare gold electrode (b) the photoiniferter modified gold electrodes.

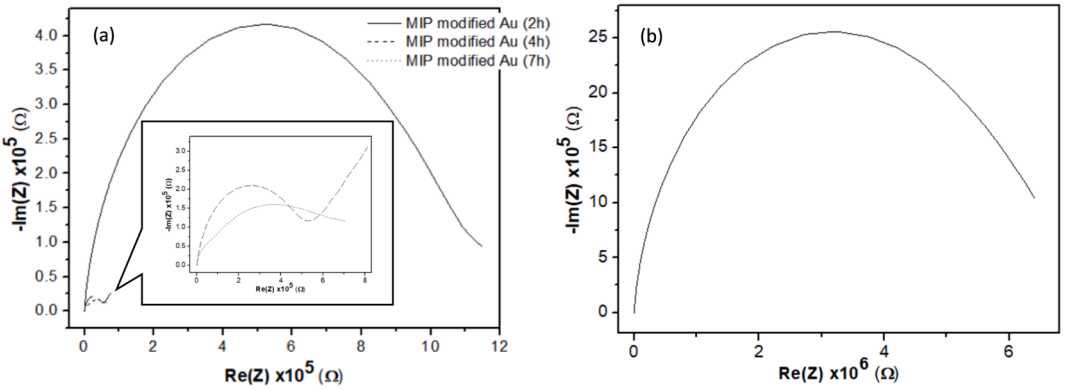


**Fig. 5.** Electrochemical impedance spectra recorded in 1 mM $[Fe(CN)_6^{4-}]/[Fe(CN)_6^{3-}]$ in 0.1 M KCl of (a) e-MIP(2 h) modified, e-MIP(4 h) modified, e-MIP(7 h) modified gold electrodes, and (b) e-NIP(4 h) modified gold electrodes.

**Table 1**
Charge-transfer resistance of bare gold electrode and the modified electrodes.

| Electrodes | Charge transfer resistance ($R_{ct}$) values (kΩ) |
|---|---|
| Bare gold electrode | **1.3** |
| Iniferter modified electrode | 805 |
| e-NIP(4 h) modified electrode | 7 109 |
| e-MIP(2 h) modified electrode | 1 097 |
| e-MIP(4 h) modified electrode | 49.4 |
| e-MIP(7 h) modified electrode | 73.6 |

investigate the charge transfer kinetics between the electrolyte and the charged ions at the electrode interface, mass transfer of ions, and electroanalytical performance of gold electrode and modified electrodes at the electrode/electrolyte interface. Fig. 4**a and b** show the impedance plots (Nyquist plots) of the bare gold electrode and the photoiniferter SAM-modified electrode respectively. It can be seen from Fig. 4**a** that the bare gold electrode showed a very small semicircle at high frequencies and a straight-line tail at low frequencies, indicating a diffusion-controlled process for the redox couple on bare gold surface. However, the impedance plot of the photoiniferter modified electrode shows a large semicircle in the entire range of frequency (Fig. 4**b**), characteristic of complete charge transfer control implying a perfect blocking behavior [31].

### 3.2. Optimization of polymerization time

Once activated by UV radiation, the photoiniferter grafted to the gold electrode surface is in charge of inducing CLRP. The advantages of using photoiniferter-mediated CLRP for MIP synthesis on a gold surface include the fabrication of uniform thin layers of MIPs providing reduced mass-transfer resistance and a uniform distribution of binding cavities. The polymerization is initiated by UV irradiation and is performed at

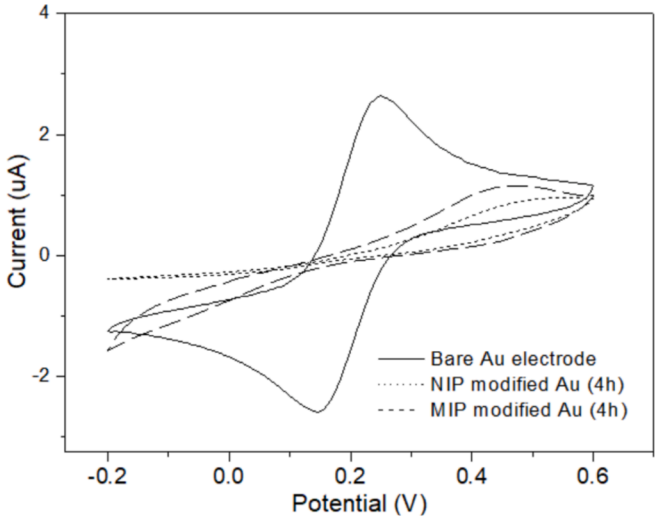


**Fig. 6.** Cyclic voltammograms carried out in 1 mM $[Fe(CN)_6^{4-}]/[Fe(CN)_6^{3-}]$ in 0.1 M KCl using bare gold e-NIP(4 h) modified gold, e-MIP(4 h) modified gold electrodes. SCE reference electrode. V = 100 mV/s.

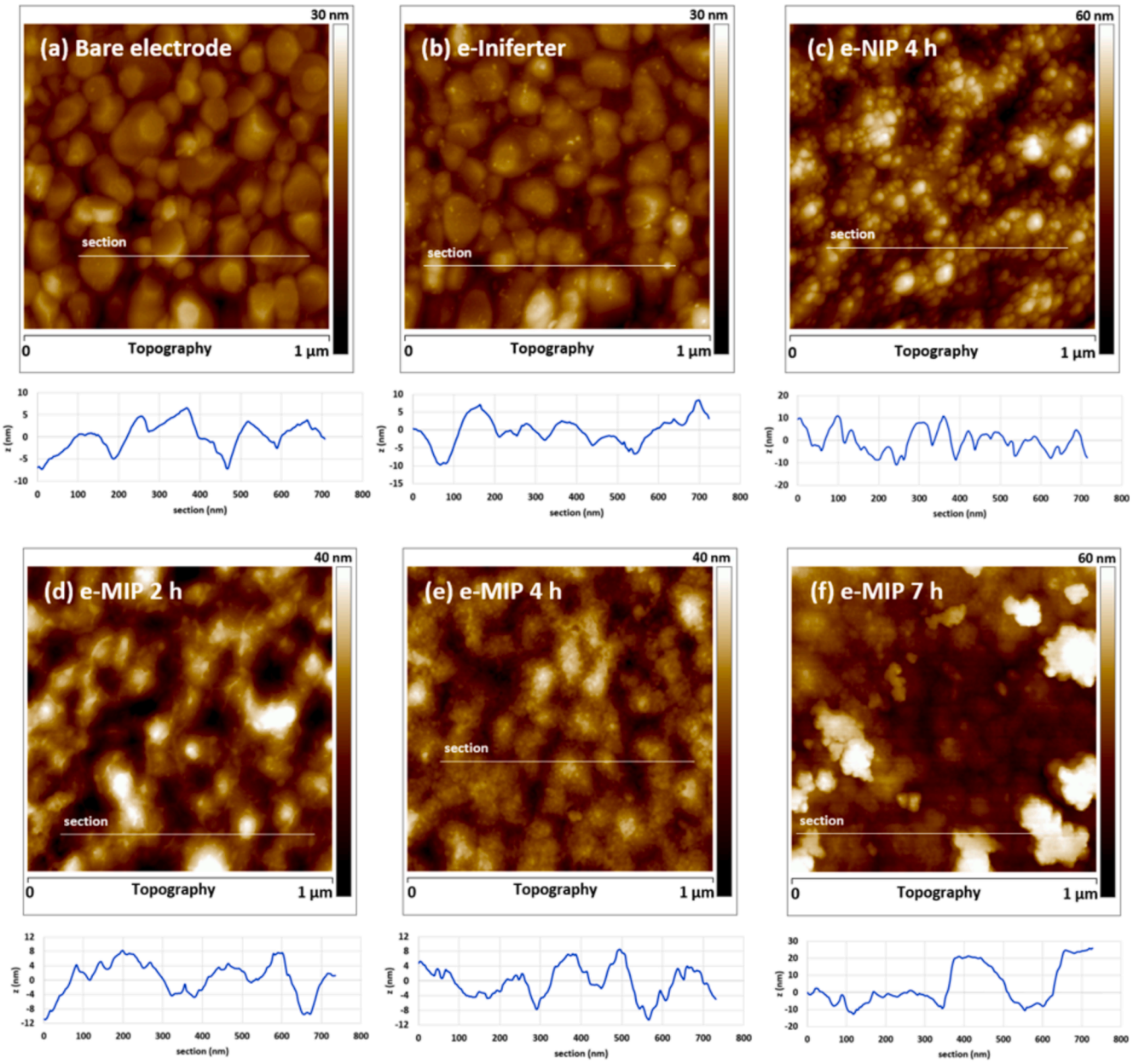


**Fig. 7.** AFM topographic images (1 µm) and corresponding cross sections of (a) bare gold electrode, (b) iniferter-modified gold electrode, (c) e-NIP (4 h) modified gold electrode, (d) e-MIP (2 h) modified gold electrode, (e) e-MIP (4 h) modified gold electrode, (f) e-MIP (7 h) modified gold electrode.

room temperature, where the template-monomer complexes are stable. Unlike traditional radical polymerization, photoinitiated CLRP can be stopped, or reinitiated, by simply turning the UV lamp off, or on. In this context, the polymer layer thickness can be optimized by controlling the polymerization time.

The coating of gold electrodes with e-MIP was monitored over time using EIS and CV. Fig. 5 shows the impedance spectra of e-MIP-modified gold electrodes after polymerization for 2 h, 4 h and 7 h. In the case of the e-MIP modified electrode after polymerization for 2 h, a large semicircle is observed highlighting a blocking behavior of the formed e-MIP layer. The e-MIP modified electrode after 4 h of polymerization showed a semicircle at high frequency region and a straight line at low frequency region, indicating a lower blocking ability and the presence of a diffusion-controlled process as for the bare electrode. When the polymerization time was extended to 7 h, the diffusion process decreased again, and the spectrum showed a distorted semi-circle. The behavior of e-NIP (4 h) was very similar, showing no diffusion and indicating that the e-NIP layer is insulative.

EIS data are commonly analyzed by fitting the data to an equivalent electrical circuit model. In the cases of bare gold surface and the e-MIP-modified electrode (4 h), the impedance data were fitted to Randles circuit [32] consisting of the solution resistance $R_s$ in series with a parallel combination of a constant phase element (*CPE*) and a series combination of charge transfer resistance, $R_{ct}$ and the Warburg impedance, *W*. For the iniferter-modified electrode, the e-MIP-modified electrode (2 h), the e-MIP (7 h), as well as the NIP-modified electrode, the Warburg impedance, *W* was not observed and a more complex behavior was observed that could not be interpreted by the Randles circuit. All the experimental EIS data obtained were fitted according to a suitable electrical equivalent circuit. The experimental and the fitted data as well as the corresponding equivalent circuit models are given in the supporting information (Table S1). Table 1 shows the charge transfer resistance values ($R_{ct}$) of the bare gold and the modified electrodes obtained from the impedance plots. The lowest charge-transfer resistance

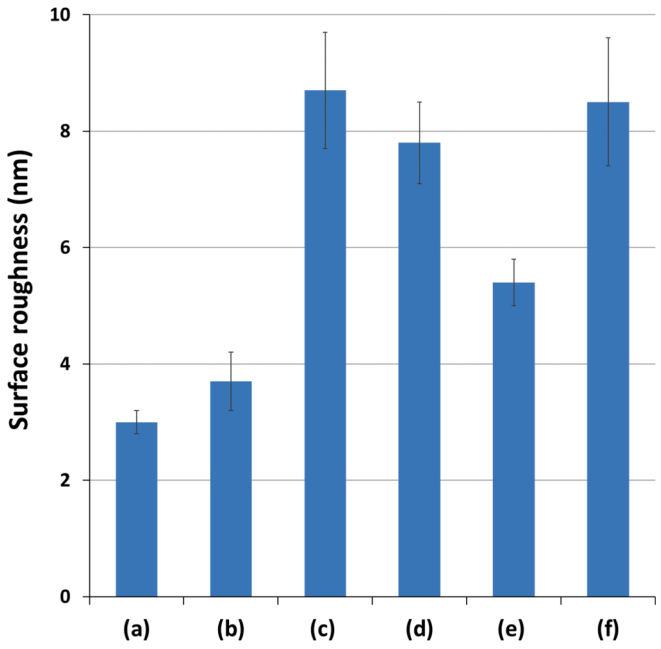


**Fig. 8.** Surface roughness (Rq) values calculated from the topographic images (1 μm) (a) bare gold electrode, (b) iniferter-modified gold electrode, (c) e-NIP (4 h) modified gold electrode, (d) e-MIP (2 h) modified gold electrode, (e) e-MIP (4 h) modified gold electrode, (f) e-MIP (7 h) modified gold electrode.

was observed for the bare gold electrode. Each subsequent modification induced an increase in this resistance due to the inhibition of the electron transfer rate by the presence of the monolayer on the electrode surface [32]. In the first stage, this increase was an evidence of the photoiniferter SAM formation, with $R_{ct}$ increasing from 1.3 kΩ to 805 kΩ. In the case of the e-NIP, the significant increase of $R_{ct}$ to 7109 kΩ indicates the formation of an insulative polymer layer that blocks the diffusion of $Fe(CN)_6^{4-}$ ions to the electrode surface. This is consistent with the absence of any binding cavities. During the e-MIP formation, a slow photopolymerization kinetics was observed in the early stage. After 2 h of polymerization, this resulted in a too limited amount of ferrocene incorporated in the polymer film, to ensure an increase in the charge transfer. However, after 4 h of polymerization, a sufficient amount of ferrocene was incorporated into the binding cavities leading to a decrease in $R_{ct}$. Extending the polymerization to 7 h produced a polymer layer too thick for efficient charge transfer. These observations are consistent with the lack of diffusive character in the electrochemical impedance spectra, except for the bare electrode and the e-MIP(4 h) layer.

Fig. 6 shows the cyclic voltammograms of the gold electrode before modification and after modification by the e-NIP and the e-MIP (4 h) using the redox $[Fe(CN)_6^{4-}]/[Fe(CN)_6^{3-}]$ couple as the external electroactive probe. As already observed in the case of the photoiniferter modified electrode, the NIP-modified and the MIP-modified electrodes lead to an important decrease of reversible redox system of $[Fe(CN)_6^{4-}]/[Fe(CN)_6^{3-}]$ couple in cyclic voltammetry compared to bare gold electrode. The reduction of the redox couple signal after polymer coating confirms the coverage of the electrode surface.

### 3.3. Physico-chemical characterization of the modified electrodes

AFM analysis was carried out to image the surface topography (1 μm × 1 μm) of the bare and modified gold electrodes (Fig. 7). The surface of the bare electrode showed clean gold granules of 50–150 nm and appeared very smooth with nanometric roughness Rq of 3.0 nm. After incubation with the photoiniferter, slight changes in surface aspect and surface roughness can be observed (Rq 3.7 nm). After surface-initiated polymerization with the e-MIP, the topography of the electrodes consisted of polymer particles deposited on the gold surface. The density of the particles remarkably increased as the polymerization time increased (Fig. 7**.d, e, f**). The formation of some aggregates at the top surface was observed at a polymerization time of 7 h (Fig. 7**f**).

In terms of surface roughness, a significant increase in the electrode roughness was observed after 2 h of polymerization with a Rq value of 7.8 nm (Fig. 8). After 4 h of polymerization, a decrease in the surface roughness was observed (5.4 nm) suggesting a more homogeneous coverage of the electrode with e-MIP film. Finally, at 7 h of polymerization, the surface roughness increased again (8.5 nm) due to the presence of polymer aggregates.

In the case of the e-NIP modified electrode, the polymer particles were more easily identified on the electrode surface as their size was bigger. e-NIP particles were larger in size than e-MIP which might be due to the pattern-free polymerization for e-NIP in which the polymerization process occurs without a template. After 4 h of polymerization, the

**Table 2**
Comparison of the performance of the sensors available in the literature with the one of this work.

| Detection technique | Sorbent | Linear range | Detection limit | Ref |
|---|---|---|---|---|
| Capacitive | MIP | 13–20 mM | 3.9 mM | [33] |
| Voltammetry | MIP | 5–100 nM and 100 nM–20 μM | 1.5 nM | [34] |
| Voltammetry | e-MIP | 0.32–3.97 μM | 90 nM | [20] |
| Voltammetry | e-MIP | 0.66–4.30 nM | 0.2 nM | This work |

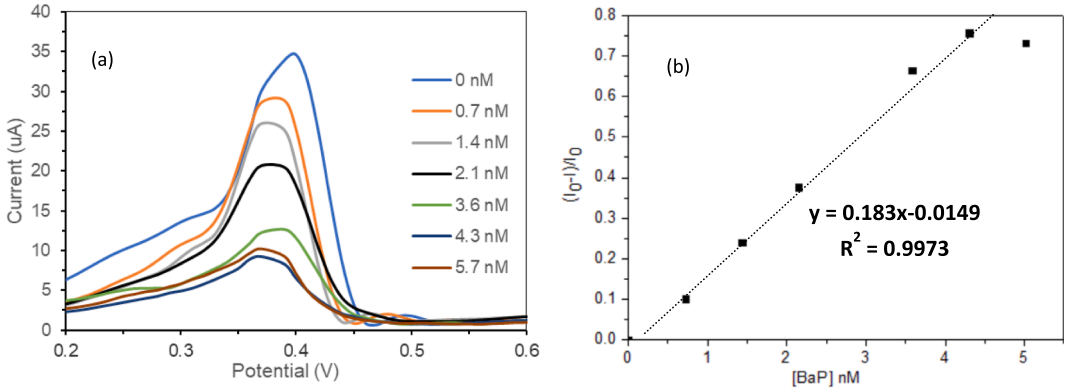


**Fig. 9.** (a) Evolution of ferrocene redox signal with BaP addition, Differential pulse voltammetry carried out in 0.1 M aqueous KCl. SCE reference electrode. V = 10 mV/s (b) Calibration curve of the e-MIP modified gold electrode.

surface roughness of the e-NIP modified electrode is measured with a Rq value of 8.7 nm. This phenomenon is consistent with the previous observation that e-NIP polymerization is faster than in the case of the e-MIP.

### 3.4. Electrochemical detection of BaP

Differential pulse voltammetry (DPV) measurements allowed to detect the ferrocene incorporated into the polymer layer in the form of FcMMA, in aqueous KCl (0.1 M). The e-MIP electrodes polymerized at different times (2 h, 4 h and 7 h) were studied. The greatest intensity of the ferrocene oxidation peak was observed in the e-MIP electrode polymerized for 4 h. Thus 4 h duration was selected as the polymerization time and the e-MIP (4 h) electrode was characterized by DPV for the electrochemical detection of BaP. However, the ferrocene oxidation peak was not detected in the case of the e-NIP (4 h) electrode. This is probably due to the insulative character of the non-imprinted polymer, which lacks diffusion enhancing vacant binding cavities. This prevents any study of the binding properties of BaP by the e-NIP electrode. For this reason, the binding properties of the e-NIP modified electrode could not be evaluated by this method.

The analytical performance of the e-MIP (4 h) electrode toward BaP detection was evaluated by addition of BaP solution aliquots to the e-MIP coated electrode. A concentration-dependent decrease in the current of the ferrocene peak was observed (Fig. 9**a**). This is due to the BaP adsorption by the e-MIP. The interaction between the BaP and the ferrocene probe of the imprinted polymer generates a shielding effect to the electron transfer on the electrode surface [20,23]. A calibration curve was obtained by plotting the relative current signal of the ferrocene oxidation *versus* the concentration of BaP. A linear correlation between the concentration and peak current was observed over the range 0.66 nM to 4.30 nM (166.52 ng/L – 1.08 μg/L) with a sensitivity of 0.18 (L $nmol^{-1}$) and a determination coefficient ($R^2$) of 0.9973 (Fig. 9**b**). The limit of detection (LOD) and limit of quantification (LOQ) were calculated using $3\sigma_b/S$ and $10\sigma_b/S$, where $\sigma_b$ is the standard deviation of the blank signal and S is the sensitivity obtained from the calibration curve slope. The LOD and LOQ recorded were 0.19 nM (47.93 ng/L) and 0.66 nM (166.52 ng/L) respectively. This procedure of electrode modification brings the recognition phase extremely close to the transducer, which we consider to be the basis of the enhanced sensitivity of the analyte.

The performance of the present electrochemical PAH molecularly imprinted material-based sensor was compared with those of sensors reported in the literature (Table 2). Its detection limit is the lowest presented so far, demonstrating an improvement over the use of carbon paste electrodes modified with BaP e-MIP particles, which had an LOD and LOQ of 90 nM (22.7 μg $L^{-1}$) and 320 nM (80.6 μg $L^{-1}$) respectively [20]. Thus, the modification of gold electrode by a e-MIP layer described in this manuscript significantly improved the sensitivity of the sensor.

## 4. Conclusions

With the aim of improving the sensitivity of electrochemical MIP as a recognition and transducer element, an e-MIP layer was grown up from the surface of a gold electrode via a “grafting from” procedure. For that purpose, a new photoiniferter was synthesized, combining a thiol group and a dithiocarbamate function. The thiol served as a linker with the gold surface to prepare a SAM which formation was evidenced by CV and EIS. The dithiocarbamate acted as an initiator for the controlled/living radical photopolymerization of the functional monomer and crosslinker to prepare the e-MIP with BaP as a marker of PAH pollutants. Ferrocenylmethyl methacrylate, used as a functional monomer to interact with BaP by π- π stacking, also played the role of redox tracer to detect BaP. In those conditions, the photoirradiation time was monitored to optimize the e-MIP layer formation, and was set to 4 h. The sensitivity of the e-MIP modified gold electrode to BaP addition was studied by DPV in KCl aqueous solution. A LOD of 0.2 nM with a linear range of 0.66 to 4.30 nM were determined. This represents a significant improvement in the performance of e-MIP-based electrodes, with a gain of a factor of 180 for the LOD compared with electrodes based on carbon paste mixed with e-MIP particles of the same composition [20]. This proves the impact of increasing the interaction between the gold electrode and the MIP, by the design of a MIP thin layer grafted to the surface of the electrode. This can be explained by a better electronic transfer between the electrode and the redox tracer. While the e-MIP modified electrode presented in this work is designed as the sensing element for the detection of BaP in aqueous samples, this concept can be extended to other families of pollutants.

## CRediT authorship contribution statement

**Farah Ibrahim:** Writing – original draft, Visualization, Investigation, Data curation. **Alexandre Sala:** Investigation. **Armand Fahs:** Investigation. **Aoife Morrin:** Writing – review & editing. **Clément Nanteuil:** Resources, Funding acquisition. **Guillaume Laffite:** Writing – review & editing, Resources. **Ian A. Nicholls:** Writing – review & editing. **Fiona Regan:** Writing – review & editing, Funding acquisition. **Hugues Brisset:** Supervision, Conceptualization. **Catherine Branger:** Writing – review & editing, Supervision, Project administration, Funding acquisition, Conceptualization.

## Declaration of competing interest

The authors declare the following financial interests/personal relationships which may be considered as potential competing interests: [Catherine Branger reports financial support was provided by French National Research Agency. Fiona Regan reports financial support was provided by Marine Institute. If there are other authors, they declare that they have no known competing financial interests or personal relationships that could have appeared to influence the work reported in this paper].

## Acknowledgements

This research was financially supported by NEMO ERANET MarTERA research program, funded by the ANR (ANR-20-MART-0001) and the Marine Institute (Ireland).

## Appendix A. Supplementary material

Supplementary data to this article can be found online at https://doi.org/10.1016/j.elecom.2024.107837.

## Data availability

Data will be made available on request.

## References

[1] H.I. Abdel-Shafy, M.S.M. Mansour, A review on polycyclic aromatic hydrocarbons: source, environmental impact, effect on human health and remediation, Egypt. J. Pet. 25 (2016) 107–123, https://doi.org/10.1016/j.ejpe.2015.03.011.
[2] S. Pavanello, M. Campisi, G. Mastrangelo, M. Hoxha, V. Bollati, The effects of everyday-life exposure to polycyclic aromatic hydrocarbons on biological age indicators, Environ. Health 19 (2020) 128–140, https://doi.org/10.1186/s12940-020-00669-9.
[3] European Community, COMMISSION REGULATION (EC) No 208/2005 of 4 February 2005 amending Regulation (EC) No 466/2001 as regards polycyclic aromatic hydrocarbons, Official Journal of the European Union (2005). https://eur-lex.europa.eu/LexUriServ/LexUriServ.do?uri=OJ:L:2005:034:0003:0005:EN:PDF.
[4] European Community, COMMISSION REGULATION (EU) No 835/2011 of 19 August 2011 amending Regulation (EC) No 1881/2006 as regards maximum levels for polycyclic aromatic hydrocarbons in foodstuffs, (2011). https://eur-lex.europa.eu/LexUriServ/LexUriServ.do?uri=OJ:L:2011:215:0004:0008:En:PDF.
[5] M. Honda, N. Suzuki, Toxicities of polycyclic aromatic hydrocarbons for aquatic animals, IJERPH 17 (2020) 1363–1385, https://doi.org/10.3390/ijerph17041363.

[6] Official Journal of the European Communities, Directive 98/83/EC on the quality of water intended for human consumption, Official Journal of the European Union 330 (1998) 32–54.
[7] European Community, Directive 2008/105/EC of the European Parliament and of the Council of 16 December 2008 on environmental quality standards in the field of water policy, amending and subsequently repealing Council Directives 82/176/EEC, 83/513/EEC, 84/156/EEC, 84/491/EEC, 86/280/EEC and amending Directive 2000/60/EC of the European Parliament and of the Council, Journal Officiel de l'Union Européenne 348 (2008) 84–97.
[8] Q. He, B. Wang, J. Liang, J. Liu, B. Liang, G. Li, Y. Long, G. Zhang, H. Liu, Research on the construction of portable electrochemical sensors for environmental compounds quality monitoring, Mater. Today Adv. 17 (2023) 100340, https://doi.org/10.1016/j.mtadv.2022.100340.
[9] J.H. Heo, M. Sung, T.Q. Trung, Y. Lee, D.H. Jung, H. Kim, S. Kaushal, N. Lee, J. W. Kim, J.H. Lee, S. Cho, Sensor design strategy for environmental and biological monitoring, EcoMat 5 (2023) e12332.
[10] A. Pandey, S. Singh, S.P. Singh, Molecularly imprinted polymers: Applications and challenges in biological and environmental sample analysis, in: Molecularly Imprinted Polymers (MIPs), Elsevier, 2023, pp. 321–344, https://doi.org/10.1016/B978-0-323-91925-8.00010-7.
[11] X. Ni, X. Tang, D. Wang, J. Zhang, L. Zhao, J. Gao, H. He, P. Dramou, Research progress of sensors based on molecularly imprinted polymers in analytical and biomedical analysis, J. Pharm. Biomed. Anal. (2023) 115659, https://doi.org/10.1016/j.jpba.2023.115659.
[12] N. Leibl, K. Haupt, C. Gonzato, L. Duma, Molecularly imprinted polymers for chemical sensing: a tutorial review, Chemosensors 9 (2021) 123, https://doi.org/10.3390/chemosensors9060123.
[13] K. Haupt, Imprinted polymers—Tailor-made mimics of antibodies and receptors, Chem. Commun. (2003) 171–178, https://doi.org/10.1039/b207596b.
[14] L. Chen, X. Wang, W. Lu, X. Wu, J. Li, Molecular imprinting: perspectives and applications, Chem. Soc. Rev. 45 (2016) 2137–2211, https://doi.org/10.1039/C6CS00061D.
[15] D. Ravina, M. Kumar, H Mohan Prasad, Biological recognition elements, in: Electrochemical Sensors, Elsevier, 2022, pp. 213–239, https://doi.org/10.1016/B978-0-12-823148-7.00008-8.
[16] K. Haupt, P.X. Medina Rangel, B.T.S. Bui, Molecularly imprinted polymers: antibody mimics for bioimaging and therapy, Chem. Rev. 120 (2020) 9554–9582, https://doi.org/10.1021/acs.chemrev.0c00428.
[17] J. Baranwal, B. Barse, G. Gatto, G. Broncova, A. Kumar, Electrochemical sensors and their applications: a review, Chemosensors 10 (2022) 363, https://doi.org/10.3390/chemosensors10090363.
[18] P.C. Ferreira, V.N. Ataíde, C.L. Silva Chagas, L. Angnes, W.K. Tomazelli Coltro, T. R. Longo Cesar Paixão, W. Reis de Araujo, Wearable electrochemical sensors for forensic and clinical applications, TrAC Trends Anal. Chem. 119 (2019) 115622, https://doi.org/10.1016/j.trac.2019.115622.
[19] R.D. Crapnell, N.C. Dempsey-Hibbert, M. Peeters, A. Tridente, C.E. Banks, Molecularly imprinted polymer based electrochemical biosensors: Overcoming the challenges of detecting vital biomarkers and speeding up diagnosis, Talanta Open 2 (2020) 100018–100027, https://doi.org/10.1016/j.talo.2020.100018.
[20] D. Udomsap, C. Branger, G. Culioli, P. Dollet, H. Brisset, A versatile electrochemical sensing receptor based on a molecularly imprinted polymer, Chem. Commun. 50 (2014) 7488–7491, https://doi.org/10.1039/C4CC02658F.
[21] V.M. Ekomo, C. Branger, R. Bikanga, A.-M. Florea, G. Istamboulie, C. Calas-Blanchard, T. Noguer, A. Sarbu, H. Brisset, Detection of Bisphenol A in aqueous medium by screen printed carbon electrodes incorporating electrochemical molecularly imprinted polymers, Biosens. Bioelectron. 112 (2018) 156–161, https://doi.org/10.1016/j.bios.2018.04.022.
[22] E. Mazzotta, A. Turco, I. Chianella, A. Guerreiro, S.A. Piletsky, C. Malitesta, Solid-phase synthesis of electroactive nanoparticles of molecularly imprinted polymers a novel platform for indirect electrochemical sensing applications, Sens. Actuat. B: Chem. 229 (2016) 174–180, https://doi.org/10.1016/j.snb.2016.01.126.
[23] D. Udomsap, H. Brisset, G. Culioli, P. Dollet, K. Laatikainen, H. Siren, C. Branger, Electrochemical molecularly imprinted polymers as material for pollutant detection, Mater. Today Commun. 17 (2018) 458–465, https://doi.org/10.1016/j.mtcomm.2018.10.019.
[24] V.M. Ekomo, C. Branger, A.-M. Gavrila, A. Sarbu, D.A. Koutsouras, C. Stolz, G. G. Malliaras, H. Brisset, Electrochemical molecularly imprinted polymers in microelectrode devices, MRS Commun. 10 (2020) 324–331, https://doi.org/10.1557/mrc.2020.29.
[25] D. Elfadil, A. Lamaoui, F. Della Pelle, A. Amine, D. Compagnone, Molecularly imprinted polymers combined with electrochemical sensors for food contaminants analysis, Molecules 26 (2021) 4607, https://doi.org/10.3390/molecules26154607.
[26] C. Unger, P.A. Lieberzeit, Molecularly imprinted thin film surfaces in sensing: chances and challenges, React. Funct. Polym. 161 (2021) 104855–104864, https://doi.org/10.1016/j.reactfunctpolym.2021.104855.
[27] K. Matyjaszewski, J. Spanswick, Controlled/Living Radical Polymerization. Handbook of Polymer Synthesis, Second Edition, CRC Press, 2004.
[28] S. Beyazit, B. Tse Sum Bui, K. Haupt, C. Gonzato, Molecularly imprinted polymer nanomaterials and nanocomposites by controlled/living radical polymerization, Prog. Polym. Sci. 62 (2016) 1–21, https://doi.org/10.1016/j.progpolymsci.2016.04.001.
[29] R.W. Nguema Edzang, M. Lejars, H. Brisset, J.-M. Raimundo, C. Bressy, RAFT-synthesized polymers based on new ferrocenyl methacrylates and electrochemical properties, RSC Adv. 5 (2015) 77019–77026, https://doi.org/10.1039/C5RA15310G.
[30] J.E. Krause, N.D. Brault, Y. Li, H. Xue, Y. Zhou, S. Jiang, Photoiniferter-mediated polymerization of zwitterionic carboxybetaine monomers for low-fouling and functionalizable surface coatings, Macromolecules 44 (2011) 9213–9220, https://doi.org/10.1021/ma202007h.
[31] V. Ganesh, S.K. Pal, S. Kumar, V. Lakshminarayanan, Self-assembled monolayers (SAMs) of alkoxycyanobiphenyl thiols on gold—A study of electron transfer reaction using cyclic voltammetry and electrochemical impedance spectroscopy, J. Colloid Interf. Sci. 296 (2006) 195–203, https://doi.org/10.1016/j.jcis.2005.08.051.
[32] V. Vivier, M.E. Orazem, Impedance analysis of electrochemical systems, Chem. Rev. 122 (2022) 11131–11168, https://doi.org/10.1021/acs.chemrev.1c00876.
[33] N.V. Beloglazova, P. Lenain, E. De Rycke, I.Y. Goryacheva, D. Knopp, S. De Saeger, Capacitive sensor for detection of benzo(a)pyrene in water, Talanta 190 (2018) 219–225, https://doi.org/10.1016/j.talanta.2018.07.084.
[34] H. Chi, Y. Li, G. Liu, A molecularly imprinted electrochemical sensor based on a $MoS_2$/peanut shell carbon complex coated with AuNPs and nitrogen-doped carbon dots for selective and rapid detection of benzo(a)pyrene, Int. J. Food Sci. Tech. 57 (2022) 5376–5387, https://doi.org/10.1111/ijfs.15869.